Fusion Energy Output Greater than the Kinetic Energy of an Imploding Shell at the National Ignition Facility

S. Le Pape,[1] L. F. Berzak Hopkins,[1] L. Divol,[1] A. Pak,[1] E. L. Dewald,[1] S. Bhandarkar,[1] L. R. Bennedetti,[1] T. Bunn,[1] J. Biener,[1] J. Crippen,[2] D. Casey,[1] D. Edgell,[3] D. N. Fittinghoff,[1] M. Gatu-Johnson,[4] C. Goyon,[1] S. Haan,[1] R. Hatarik,[1] M. Havre,[2] D. D-M. Ho,[1] N. Izumi,[1] J. Jaquez,[2] S. F. Khan,[1] G. A. Kyrala,[5] T. Ma,[1] A. J. Mackinnon,[1] A. G. MacPhee,[1] B. J. MacGowan,[1] N. B. Meezan,[1] J. Milovich,[1] M. Millot,[1] P. Michel,[1] S. R. Nagel,[1] A. Nikroo,[1] P. Patel,[1] J. Ralph,[1] J. S. Ross,[1] N. G. Rice,[2] D. Strozzi,[1] M. Stadermann,[1] P. Volegov,[5] C. Yeamans,[1] C. Weber,[1] C. Wild,[6] D. Callahan,[1] and O. A. Hurricane[1]

[1]*Lawrence Livermore National Laboratory, Livermore, California 94550, USA*
[2]*General Atomics, San Diego, California 92186, USA*
[3]*Laboratory for Laser Energetics, University of Rochester, Rochester, New York 14636, USA*
[4]*Plasma Science and Fusion Center, Massachusetts Institute of Technology, Cambridge, Massachusetts 02139, USA*
[5]*Los Alamos National Laboratory, Los Alamos, New Mexico 87545, USA*
[6]*Diamond Materials Gmbh, 79108 Freiburg, Germany*

(Received 3 November 2017; revised manuscript received 4 May 2018; published 14 June 2018)

A series of cryogenic, layered deuterium-tritium (DT) implosions have produced, for the first time, fusion energy output twice the peak kinetic energy of the imploding shell. These experiments at the National Ignition Facility utilized high density carbon ablators with a three-shock laser pulse (1.5 MJ in 7.5 ns) to irradiate low gas-filled (0.3 mg/cc of helium) bare depleted uranium hohlraums, resulting in a peak hohlraum radiative temperature ~290 eV. The imploding shell, composed of the nonablated high density carbon and the DT cryogenic layer, is, thus, driven to velocity on the order of 380 km/s resulting in a peak kinetic energy of ~21 kJ, which once stagnated produced a total DT neutron yield of 1.9×10^{16} (shot N170827) corresponding to an output fusion energy of 54 kJ. Time dependent low mode asymmetries that limited further progress of implosions have now been controlled, leading to an increased compression of the hot spot. It resulted in hot spot areal density ($\rho r \sim 0.3$ g/cm^2) and stagnation pressure (~360 Gbar) never before achieved in a laboratory experiment.

DOI: 10.1103/PhysRevLett.120.245003

The potential of nuclear fusion as an efficient source of energy was identified decades ago [1]. However, harnessing fusion for energy production has proven to be a difficult task. Throughout the world, billions of dollars are invested in experimental facilities and programs with the goal of demonstrating ignition—the point at which the amount of energy produced via fusion reactions is equal to or greater than the energy supplied to initiate the process [2]. At Lawrence Livermore National Laboratory, the indirect drive approach for inertial confinement fusion (ICF) is pursued at the National Ignition Facility (NIF) [3]. Most ICF work on the NIF is based on the hot spot ignition concept, where the kinetic energy of an imploding shell is converted, upon stagnation, to internal energy in a central hot spot. Fusion is initiated in the hot spot, and a thermonuclear burn front propagates radially outward into the main fuel producing high gain if the main fuel is of sufficiently high areal density. Ignition is only achieved when self-heating of the hot spot occurs: 3.5 MeV α particles produced by the deuterium-tritium (DT) fusion reactions transfer their energy to the central hot spot to compensate for bremsstrahlung, conduction, and any other energy losses. The theoretical fusion yield can be in the megajoule range, exceeding by a factor of 1000 the kinetic energy supplied to the deuterium-tritium fuel by the implosion alone. While megajoule fusion yields are the goal of the ICF program, reaching that stage requires achieving distinct steps in target gain and yield, each representative of the understanding and resolution of key issues.

The high foot design, in reducing the implosion vulnerability to hydrodynamic instabilities plaguing low adiabat implosions, achieved a net fuel gain (as defined in Ref. [4]) in a hot spot dominated by alpha heating [5]. Nevertheless, the high foot implosions plateaued near 26 kJ of fusion yield, hot spot areal density < 0.2 g/cm^2 and 250 Gbar of stagnation pressure. Detailed analyses have shown that symmetry swings were, in part, responsible for the implosion degradation [6] and the high apparent ion temperature measured [7,5].

The high density carbon (HDC) experiments we report on, by controlling low mode asymmetry through the laser history, achieved, for the first time, a fusion yield (54 kJ)

twice the kinetic energy of the imploding shell ($E_K \sim 21$ kJ $\pm$ 5 kJ)

$$E_K = \frac{1}{2}(M_{\mathrm{HDC}} + M_{\mathrm{DT}})V_{\mathrm{imp}}^2. \quad (1)$$

Where the mass of the DT cryogenic layer M_{DT} is 0.13 mg, the mass of the nonablated HDC M_{HDC} is 0.13 mg $\pm$ 0.03, and the maximum implosion velocity V_{imp} is 380 km/cm $\pm$ 30.

At a similar adiabat to the high foot campaign, the HDC approach of minimizing low mode asymmetry of the x-ray drive throughout the implosion history [8,9] led to a hot spot ρr (~0.3 g/cm^2), high enough to stop most (~85%) of the α particles. The hot spot areal density is now high enough (see Fig. 4) to sustain self heating once the confinement time is increased. The energy deposited by the α particle in the hot spot is now ~10 kJ, more than twice the α deposited energy of any previous experiment [5]. Furthermore, the stagnation pressure of the hot spot (~360 Gbar) is now higher than the pressure of the solar core [10].

Consequently, the conditions achieved in the hot spot now enable access to a range of nuclear and astrophysical regimes. The density, temperature, and pressure of the hot spot are the closest on earth to conditions in the sun [11,12], and the neutron density ($> 10^{23}$ neutron/cc) is now relevant for nucleosynthesis studies (such as the s process), which have traditionally been in need of an intense, laboratory-based neutron source [13,14].

To reach these hot spot conditions, the shell has to implode nearly spherically at all times [15]. The HDC shell sits at the center of a high-Z cylinder ("hohlraum") irradiated by the 192 NIF laser beams, the symmetry of the x-ray radiation bath resulting from the interaction of the laser beams with the hohlraum walls dictates the symmetry of the imploding shell. The use of HDC ablators [16–18] has enabled us to lower x-ray drive asymmetries. Thin (70 μm) HDC ablators permit the usage of shorter laser pulses (< 9 ns), facilitating symmetry control as the hohlraum fills over time with expanding high-Z plasma from the hohlraum wall (bare depleted uranium in this Letter).

The implosion symmetry is controlled throughout the laser drive history by adjusting the relative power balance between the inner and outer laser cones. Following the methodology described in [8] using a 5.75 m diameter hohlraum and a 844 μm inner radius (scale 5.75) HDC shell, the implosion symmetry was measured and optimized at the larger 6.2 scale (Fig. 1). Figure 2 provides an overall quantitative view of symmetry measurements obtained at different times and convergences using multiple experimental platforms [two axis keyhole [19], 2D radiograph of the in-flight compressed shell [20], low convergence gas-filled capsule ("Symcap") [21], and high convergence cryogenic DT layer [22]]. At all times along the shell

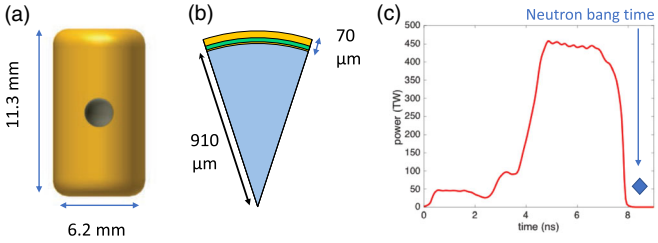

FIG. 1. Target and laser specifications for shots N170601 and N170827. (a) 6.20 mm scale hohlraum (b) 70 μm thick HDC capsule used in the 6.20 mm scale hohlraum, green layer denotes the doped layer. This figure illustrates the doped layer of the HDC capsule. The doped HDC layer is 20 microns thick doped with 0.3% atomic percent of tungsten to shield the fuel from suprathermal x rays. This shielding is designed to reduce decompression of the inner capsule region and fuel and to improve the stability of the fuel-capsule interface. (c) Laser pulse.

trajectory, symmetry is controlled to better than ± 10 μm; the hot spot at bang time is within 6 μm of round.

Following this series of symmetry experiments, two cryogenic DT layered experiments (shots N170601 and N170827) were carried out to test fusion performance at high convergence. The hohlraum was driven to ~290 eV radiation temperature by 1.5 and 1.7 MJ of laser energy at 450 TW peak power [Fig. 1(c)]. Figure 3 shows equatorial and polar images of the measured primary neutron emission

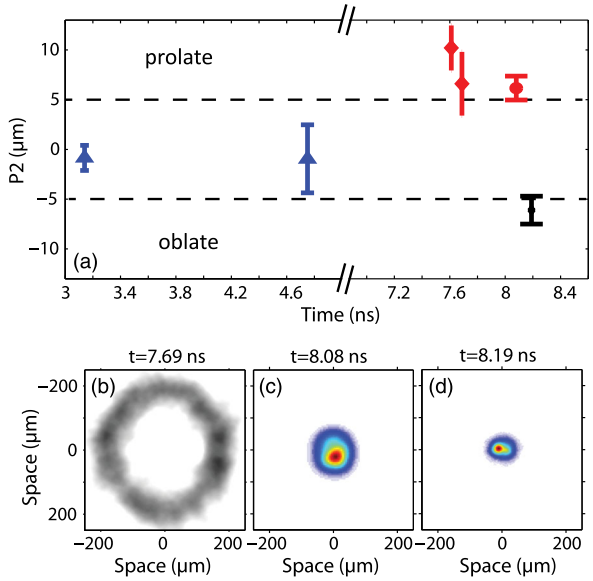

FIG. 2. (a) History of the implosion symmetry for the doped HDC capsule measured at increasing convergence and time using a succession of experimental techniques. Blue points are keyhole data, red points are 2DconA data, black point is the DT cryogenic platform. The definition of $P2$ in microns as a measure of deviation from round is described in the text. (b) equatorial x-ray radiograph of the shell, (c) equatorial x-ray image of the hot spot at bang time (convergence 17) (d), equatorial x-ray image of the hot spot at bang time (convergence 25).

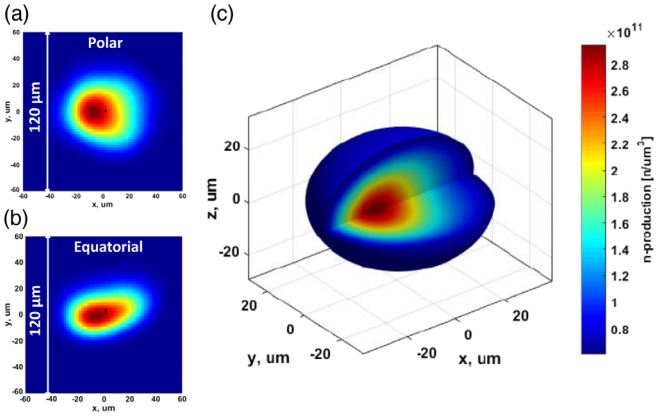

FIG. 3. Shot N170601. (a) Polar neutron image. (b) Equatorial neutron image. (c) Three-dimensional reconstructed neutron volume of the hot spot.

(12–15 MeV) as well as the reconstructed neutron production volume at bang time [23] for N170601 (N170827 has a similar hot spot shape and volume). The neutron volume is slightly ellipsoidal, with a measured $P2$ of -6 ± 2 μm, (as fit with the second Legendre moment, $P2$).

Table I summarizes the results of these two shots (N170601 and N170827) and, for comparison, one of the best performers of the high foot campaign (shot N140304) [24]. The high foot campaign is a high adiabat campaign based on a Plastic (CH) ablator, that reached the α heating regime by reducing the impact of hydrodynamic instabilities on the hot spot compression [5,25]. Neutron yield, down scatter ratio (DSR) and DT ion temperature shown in Table I are directly measured by neutron time of flight (NTOF) detectors [26]. Quantities such as hot spot ρr, hot spot energy, stagnation pressure and α deposited energy are inferred from experimental observables using a "hot spot" model described in [27].

The total neutron yield is derived from the measured primary neutron yield and DSR using the relation $\text{yield}_{\text{total}} = \text{yield}_{13\text{–}15\ \text{Mev}} e^{4\,\text{DSR}}$ [28]. The hot spot density is then derived from the measured yield, burn width, and neutron volume using the relation [4]

$$Y = \langle \sigma V \rangle \tau V_{\text{hs}} N_D N_T, \tag{2}$$

where $\langle \sigma V \rangle$ is the equimolar DT reactivity, which is a function of the ion temperature. V_{hs} is the volume of neutron emission, which is calculated using the equatorial and polar neutron images, and τ is the neutron burn width measured by the gamma reaction history detector [29]. The hot spot stagnation pressure is inferred from the hot spot density and ion temperature measured by the NTOF detectors using the relation $P_{\text{stag}} = [(\bar{Z}+1)/\bar{A}m_p]\rho T_{\text{ion}}$, where $\bar{Z} = 1$ for DT, $\bar{A} = 2.5$ is the average atomic mass number. This leads to the determination of the hot spot energy using the relation $E_{\text{hs}} = 3/2 P_{\text{stag}} V_{\text{hs}}$.

To infer the energy deposited by α particles, the fraction of α energy deposited f_α, assuming a spherical hot spot, is first calculated. It is a function of the hot spot ρr and ion temperature [30]

$$f_\alpha = 1 - \frac{1}{4[(\rho r)_{\text{hs}}/\rho\lambda_\alpha]} + \frac{1}{160[(\rho r)_{\text{hs}}/\rho\lambda_\alpha]^3}, \tag{3}$$

where the α particle stopping range is

$$\rho\lambda_\alpha = \frac{0.025 T_e^{5/4}}{1 + 0.0082 T_e^{5/4}}, \tag{4}$$

where T_e is the electron temperature, assuming $T_e = T_i$, in base units of centimeters, grams, and kiloelectronvolts.

The energy partition in a DT fusion event is 80% to a 14.1 MeV neutron and 20% to a 3.5 MeV α particle. Therefore, the energy deposited by an α particle in the hot spot can be derived from the fraction of α deposited energy and the total fusion yield.

TABLE I. Summary of experimental data from cryogenic DT layer implosions at 6.20 scale (N170601, N170827) and for a high performance high foot experiment (N140304).

	N170601 data	N170827 data	N140304 data
Total neutron yield	$1.7e16 \pm 2.4e14$	$1.9e16 \pm 3e14$	$9.3e15 \pm 1.7e14$
Fusion yield (kJ)	48	53	26
DT Tion (keV)	4.5 ± 0.12	4.5 ± 0.15	5.5 ± 0.12
DSR (%)	3.27 ± 0.2	3.24 ± 0.2	3.4 ± 0.20
Velocity (km/s)	381	395	380
Pstag (Gbar)	320 ± 40	360 ± 45	222 ± 15
Nuclear burn width (ps)	160 ± 30	154 ± 30	163 ± 30
Hot spot $\rho * r$ (g/cm^2)	0.26 ± 0.032	0.30 ± 0.034	0.13 ± 0.021
α deposited fraction f_α	0.81	0.87	0.58
Hot spot energy (kJ)	4.3 ± 1.17	4.7 ± 1.7	3.6 ± 1.03
Shell max kinetic energy (kJ)	22 ± 5	21 ± 5	25 ± 7
Alpha deposited energy (kJ)	8 ± 1.36	9.3 ± 1.6	3.3 ± 0.58

A key achievement of the high foot campaign in 2014 was to achieve a fuel gain of unity: more fusion energy was produced in the hot spot than energy was delivered to the DT fuel. This demonstration required a detailed estimate of the energy balance during stagnation. Here, we have improved the implosion enough to report a net gain of two between the fusion energy produced and the maximum kinetic energy of the imploding shell, including both the DT fuel and the remaining ablator, at peak implosion velocity when the hohlraum does not accelerate the capsule anymore. This can be thought of as the fusion gain of an isolated system (the free-falling imploding shell) and reporting the gain does not have to rely on internal mechanics. The shell velocity is measured using the 2DconA platform (N170419 shot), the position of the shell is recorded as a function of time on an x-ray gated imager. The fraction of nonablated carbon at peak velocity is calculated by HYDRA and consistent with in-flight x-ray radiography. For N170827, the fusion energy (54 kJ) is more than twice the maximum kinetic energy of the imploding shell (21 kJ, see before for details), while for one of the high performing implosions, N140304, the output energy is about equal to the maximum kinetic energy of the imploding shell (see Table I).

As a result of reducing the symmetry swing in the x-ray drive, the improved compression increased the hot spot ρr by more than 50% and stagnation pressure by more than 60%. In addition to twice the fusion yield, the energy deposited by the α particle in the hot spot increased from ~3.4 kJ to ~9.7 kJ. For N170827, with a hot spot ρr of 0.3 g/cm^2 and a $T_{\rm ion}$ of 4.7 keV, $f_\alpha \sim 0.87$ which implies that the bulk of the α particles are stopped in the hot spot.

A static, isobaric hot spot model [4] can be used to estimate the energy balance in the hot spot at peak compression. The self heating condition for an isobaric hot spot can be written

$$(A_\alpha \langle \sigma v \rangle f_\alpha - A_b T^{1/2})(\rho r)^2 - \frac{3 c_e A_e T^{7/2}}{\ln \Lambda} > 0, \quad (5)$$

where $\langle \sigma v \rangle$ is the DT reactivity, f_α is the fraction of α energy deposited, $A_\alpha = 8.1 \times 10^{40}$ erg/g^2, $A_b = 3.5 \times 10^{23}$ erg.g^{-2} cm^3 s^{-1}, T is the ion temperature, ρr is the areal density in g/cm^2, ln Λ is equal to 3.7 in our hot spot conditions, $c_e = 1$, $A_e = 9.5 \times 10^{19}$ erg.keV$^{-7/2}$ cm^{-1} s^{-1}. The first term in equation (5) is the deposited fusion power; the second term is the bremsstrahlung emission power density, and the thermal conduction power density is the third term.

At the conditions achieved on N170827, bremsstrahlung and electron conduction losses are still dominating the alpha deposited energy. We can estimate from N170827 conditions (at constant ρr and adiabat) what it would take to reach equilibrium and the onset of the burning plasma regime. At constant ρr, the α deposited energy scales like $\langle \sigma v \rangle$, which roughly scales like $T_{\rm ion}^4$ [4], thus, the equilibrium is reached for an ion temperature of 4.8 keV, corresponding to a neutron yield of 2.4×10^{16}. The two solid lines shown in Fig. 4 are the yield extrapolation at constant ρr for the best high foot and HDC shots based on the DT cross section dependence with temperature. The black diamond shows the point on the yield/ion temperature curve where the α deposited energy equals the bremsstrahlung and electron conduction losses. For the best HDC shot to date, the hot spot ρr is high enough at moderate temperature (~4.7 keV) that the α deposited energy clearly exceeds the conduction losses leading to equilibrium as the ion temperature increases. At $\rho r < 0.18$ g/cm^2, the α deposited energy is never enough to compensate for the bremsstrahlung and electron conduction losses.

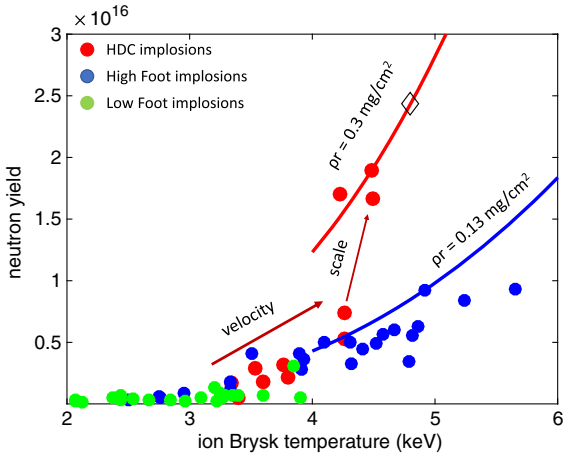

FIG. 4. Total DT neutron yield as a function of ion temperature, red dots are doped HDC implosions, blue dots are high foot implosions, green dots are low foot implosions. The neutron yield is plotted against the lowest burn averaged DT ion temperature measured by NTOF detectors (Brysk temperature). For high foot implosions, the Brysk temperature is estimated to be up to a keV higher due to flows in the hot spot. Black diamond is the point where α deposited energy equals bremsstrahlung and conduction losses. Solid curves are a yield extrapolation with temperature using a constant ρr and adiabat.

Figure 4 shows most of the cryogenic DT layered implosions carried out on the NIF since the beginning of the National Ignition Campaign [31]. The performance of HDC implosions was improved, first, by increasing the implosion velocity and, second, by increasing the target scale and shortening the time between the end of the laser pulse and the time of peak neutron emission. At scale 5.75, increasing the implosion velocity resulted in higher ion temperature and, thus, implosion performance with a velocity scaling consistent with scaling of previous high foot experiments [32]. At scale 5.75, 20 kJ of fusion yield was achieved using "only" 1.1 MJ of laser light (versus 1.7 MJ of laser light for a similar high foot implosion). To increase the performance of the HDC design further, the target size was scaled up by 8% from 5.75 to 6.20.

In addition to the power and pulse duration increase, the capsule drive was modified to reduce the time between the end of the laser and the peak neutron emission ("coast time") [Fig. 1(c)]. A reduced coast time was demonstrated to increase stagnation pressure and yield for high foot implosions [33]. These modifications led to record fusion yields and hot spots ρr shown in Fig. 4 (red dots).

Experimental yield data are 30%–50% of axisymmetric (2D) HYDRA [34] radiation hydrodynamic simulations including α deposition. The main source of yield degradation for these implosions is believed to be induced by the fill tube. The fill tube can inject, mix, and create local ρr distortion of the shell. To bring simulations in closer agreement with experimental data, mix (i.e., carbon with 0.33% atomic fraction of tungsten) can be uniformly injected in a capsule-only calculation. Typically, 50–100 ng of injected material is needed to reproduce the measured implosion performances.

The HDC campaign has produced, for the first time, a fusion energy (54 kJ) twice the peak kinetic energy of the imploding shell (21 kJ). The implosion performance was improved from previous campaigns on the NIF by lowering x-ray drive asymmetry on the imploding shell. A hot spot areal density of 0.3 g/cm^2 was achieved, high enough to stop ~85% of the α particles. The conditions in the hot spot with stagnation pressures of ~360 Gbar, greater than the solar core pressure, is attracting a new community of scientists studying nucleosynthesis on the NIF. Future shots in the campaign will aim at increasing the hot spot ion temperature by increasing the implosion velocity and further improving the shell areal density to improve the hot spot confinement.

We thank J. Edwards, N. Abbas, W. Hsing, O. L. Landen, and J. Kilkenny for enabling this research and fruitful discussions. This work was performed under the auspices of the U.S. Department of Energy by Lawrence Livermore National Laboratory under Contract No. DE-AC52-07NA27344. Work was also supported by the Laboratory Directed Research and Development Grant No. 11-ERD-050 and the National Laboratory User Facility and by General Atomics under Contract No. DE-NA0001808.

[1] J. Nuckolls, L. Wood, A. Thiessen, and G. Zimmerman, Nature (London) **239**, 139 (1972).
[2] K. A. Brueckner and S. Jorna, Rev. Mod. Phys. **46**, 325 (1974).
[3] E. I. Moses, R. N. Boyd, B. A. Remington, C. J. Keane, and R. Al-Ayat, Phys. Plasmas **16**, 041006 (2009).
[4] S. Atzeni and M. ter Vehn, *The Physics of Inertial Fusion Beam Plasma Interaction, Hydrodynamics, Dense Plasma Physics* (Clarendon Press, Oxford, 2004).
[5] O. A. Hurricane, D. A. Callahan, D. T. Casey, E. L. Dewald, T. R. Dittrich, T. Doppner, S. Haan, D. E. Hinkel, L. F. B. Hopkins, O. Jones *et al.*, Nat. Phys. **12**, 800 (2016).
[6] A. L. Kritcher, D. E. Hinkel, D. A. Callahan, O. A. Hurricane, D. Clark, D. T. Casey, E. L. Dewald, T. R. Dittrich, T. Doppner, M. A. B. Garcia *et al.*, Phys. Plasmas **23**, 052709 (2016).
[7] M. G. Johnson, J. P. Knauer, C. J. Cerjan, M. J. Eckart, G. P. Grim, E. P. Hartouni, R. Hatarik, J. D. Kilkenny, D. H. Munro, D. B. Sayre *et al.*, Phys. Rev. E **94**, 021202 (2016).
[8] L. Divol, A. Pak, L. F. B. Hopkins, S. L. Pape, N. B. Meezan, E. L. Dewald, D. D. -M. Ho, S. F. Khan, A. J. Mackinnon, J. S. Ross *et al.*, Phys. Plasmas **24**, 056309 (2017).
[9] B. Cheng, T. J. T. Kwan, Y.-M. Wang, and S. H. Batha, Phys. Rev. E **88**, 041101 (2013).
[10] J. Christensen-Dalsgaard and G. Berthomieu, in *Solar Interior and Atmosphere*, edited by A. Cox, W. Livingston, and M. Matthews (University of Arizona Press, Tucson, 1991), pp. 401–478.
[11] R. N. Boyd, L. A. Bernstein, and C. Brune, Phys. Today **62**, 60 (2009).
[12] D. A. Shaughnessy, N. Gharibyan, K. J. Moody, J. D. Despotopulos, P. M. Grant, C. B. Yeamans, L. B. Hopkins, C. J. Cerjan, D. H. G. Schneider, and S. Faye, J. Phys. Conf. Ser. **717**, 012080 (2016).
[13] A. Frebel and T. Beers, Phys. Today **71**, 30 (2018).
[14] The neutron fluxes reported in the Letter would allow the measurement of neutron capture by unstable nucleides. Tm-171, due to its importance as a branching point nucleus in the slow process (*s* process), has been proposed for an experiment on the NIF. Its relatively short half-life renders measurements at accelerator-based neutron irradiation facilities (such as LANSCE) extremely challenging. Adding 10 ng of TM-171 in the HDC ablator would produce ~10^7 atoms of Tm172 that could be captured by the NIF Solid Radiochemistry Diagnostics.
[15] A. L. Kritcher, R. Town, D. Bradley, D. Clark, B. Spears, O. Jones, S. Haan, P. T. Springer, J. Lindl, R. H. H. Scott *et al.*, Phys. Plasmas **21**, 042708 (2014).
[16] J. Biener, D. Ho, C. Wild, E. Woerner, M. Biener, B. El-dasher, D. Hicks, J. Eggert, P. Celliers, G. Collins *et al.*, Nucl. Fusion **49**, 112001 (2009).
[17] A. J. MacKinnon, N. B. Meezan, J. S. Ross, S. L. Pape, L. B. Hopkins, L. Divol, D. Ho, J. Milovich, A. Pak, J. Ralph *et al.*, Phys. Plasmas **21**, 056318 (2014).
[18] D. D. -M. Ho, S. W. Haan, J. D. Salmonson, D. S. Clark, J. D. Lindl, J. L. Milovich, C. A. Thomas, L. F. B. Hopkins, and N. B. Meezan, J. Phys. Conf. Ser. **717**, 012023 (2016).
[19] J. D. Moody, H. F. Robey, P. M. Celliers, D. H. Munro, D. A. Barker, K. L. Baker, T. Doppner, N. L. Hash, L. B. Hopkins, K. LaFortune *et al.*, Phys. Plasmas **21**, 092702 (2014).
[20] J. R. Rygg, O. S. Jones, J. E. Field, M. A. Barrios, L. R. Benedetti, G. W. Collins, D. C. Eder, M. J. Edwards, J. L. Kline, J. J. Kroll *et al.*, Phys. Rev. Lett. **112**, 195001 (2014).
[21] G. A. Kyrala, J. L. Kline, S. Dixit, S. Glenzer, D. Kalantar, D. Bradley, N. Izumi, N. Meezan, O. Landen, D. Callahan *et al.*, Phys. Plasmas **18**, 056307 (2011).

[22] S. H. Glenzer, D. A. Callahan, A. J. MacKinnon, J. L. Kline, G. Grim, E. T. Alger, R. L. Berger, L. A. Bernstein, R. Betti, D. L. Bleuel *et al.*, Phys. Plasmas **19**, 056318 (2012).
[23] P. Volegov, C. R. Danly, D. N. Fittinghoff, G. P. Grim, N. Guler, N. Izumi, T. Ma, F. E. Merrill, A. L. Warrick, C. H. Wilde *et al.*, Rev. Sci. Instrum. **85**, 023508 (2014).
[24] T. Doppner, D. A. Callahan, O. A. Hurricane, D. E. Hinkel, T. Ma, H.-S. Park, L. F. B. Hopkins, D. T. Casey, P. Celliers, E. L. Dewald *et al.*, Phys. Rev. Lett. **115**, 055001 (2015).
[25] T. R. Dittrich, O. A. Hurricane, D. A. Callahan, E. L. Dewald, T. Döppner, D. E. Hinkel, L. F. B. Hopkins, S. Le Pape, T. Ma, J. L. Milovich *et al.*, Phys. Rev. Lett. **112**, 055002 (2014).
[26] R. A. Lerche, V. Y. Glebov, M. J. Moran, J. M. McNaney, J. D. Kilkenny, M. J. Eckart, R. A. Zacharias, J. J. Haslam, T. J. Clancy, M. F. Yeoman *et al.*, Rev. Sci. Instrum. **81**, 10D319 (2010).
[27] O. A. Hurricane, D. A. Callahan, D. T. Casey, P. M. Celliers, C. Cerjan, E. L. Dewald, T. R. Dittrich, T. Doppner, D. E. Hinkel, L. F. B. Hopkins *et al.*, Nature (London) **506**, 343 (2014).
[28] D. T. Casey, J. A. Frenje, M. G. Johnson, F. H. Sguin, C. K. Li, R. D. Petrasso, V. Y. Glebov, J. Katz, J. Magoon, D. D. Meyerhofer *et al.*, Rev. Sci. Instrum. **84**, 043506 (2013).
[29] H. W. Herrmann, N. Hoffman, D. C. Wilson, W. Stoeffl, L. Dauffy, Y. H. Kim, A. McEvoy, C. S. Young, J. M. Mack, C. J. Horsfield *et al.*, Rev. Sci. Instrum. **81**, 10D333 (2010).
[30] O. N. Krokhin and V. B. Rozanov, Sov. J. Quantum Electron. **2**, 393 (1973).
[31] J. Lindl, O. Landen, J. Edwards, and E. Moses, Phys. Plasmas **21**, 020501 (2014).
[32] D. A. Callahan, O. A. Hurricane, D. E. Hinkel, T. Doppner, T. Ma, H.-S. Park, M. A. B. Garcia, L. F. B. Hopkins, D. T. Casey, C. J. Cerjan *et al.*, Phys. Plasmas **22**, 056314 (2015).
[33] O. A. Hurricane, A. Kritcher, D. A. Callahan, O. Landen, P. K. Patel, P. T. Springer, D. T. Casey, E. L. Dewald, T. R. Dittrich, T. Doppner *et al.*, Phys. Plasmas **24**, 092706 (2017).
[34] M. M. Marinak, G. D. Kerbel, N. A. Gentile, O. Jones, D. Munro, S. Pollaine, T. R. Dittrich, and S. W. Haan, Phys. Plasmas **8**, 2275 (2001).